INTERNATIONAL JOURNAL OF HYDROGEN ENERGY 47 (2022) 39678–39686

Available online at www.sciencedirect.com

ScienceDirect

journal homepage: www.elsevier.com/locate/he

Short Communication

A comparative study of the catalytic performance of nickel supported on a hibonite-type La-hexaaluminate synthesized from aluminum saline slags in the dry reforming of methane

*J.J. Torrez-Herrera, S.A. Korili, A. Gil**

INAMAT2-Departamento de Ciencias, Edificio de los Acebos, Universidad Pública de Navarra, Campus de Arrosadía, E-31006, Pamplona, Spain

HIGHLIGHTS

- Acid aluminum extracted was used in the synthesis of a La-hexaaluminate.
- The solid was used as support for Ni catalyst for DRM.
- Three Ni-catalysts from commercial supports were used for comparison.
- The behavior of Ni/LHA is similar to the catalysts with high Ni-support interaction.

ARTICLE INFO

Article history:
Received 2 July 2022
Received in revised form
9 September 2022
Accepted 13 September 2022
Available online 30 September 2022

Keywords:
Aluminum industrial waste valorization
Hexaaluminate synthesis from aluminum saline slags
Nickel supported hexaaluminate
Dry reforming of methane

ABSTRACT

In this work, a hibonite-type Ni/La-hexaaluminate (Ni/LHA) synthesized from an industrial waste is used and compared as catalyst in the dry reforming of methane (DRM) at 973 K. The structure, catalytic behavior, and stability during a run time of at least 50 h of three Ni-catalysts obtained from two commercial supports and two preparation methods were used for comparison. An aluminum solution (9.40 g/L) obtained from an aluminum saline slag waste by acid extraction was used to synthesize the hexaaluminate by mixing with a stoichiometric amount of lanthanum nitrate and methanol/Peg400/PegMn400 under hydrothermal conditions at 493 K for 16 h. The Ni/LHA catalyst (10 wt% NiO) was obtained by impregnation of the synthesized support, calcined previously at 1473 K for 2 h. The resulting solids were characterized by several techniques as: X-ray diffraction (XRD), N_2 adsorption at 77 K, temperature-programmed reduction (TPR), scanning electron microscopy (SEM) and transmission electron microscopy (HR-TEM). In order to compare the catalytic behavior and properties of the Ni/LHA catalyst, three Ni catalysts obtained from two commercial supports (γ-Al_2O_3 and SiO_2) and two preparation methods (wet impregnation (I) and precipitation-deposition (PD)) were synthesized. Analysis of the TPR patterns for the catalysts allowed the type of metal support interaction and NiO species to be determined, with a weak interaction with the support being observed in Ni/LHA and Ni–I/SiO_2. The NiO species observed, with crystallite sizes between 9.7 and 40.4 nm, confirm the X-ray structural analyses. The Ni/LHA catalyst was found to be active and very stable in the DRM reaction after 50 h. The catalytic behavior was evaluated from the CO_2 and CH_4

* *Corresponding author.*
E-mail address: andoni@unavarra.es (A. Gil).
https://doi.org/10.1016/j.ijhydene.2022.09.131

conversions, as well as the H_2/CO selectivity, with values of 99% over almost all the time range evaluated. The behavior of this catalyst is comparable to that of Ni–I/Al_2O_3 and Ni-PD/SiO_2. The results found indicating that the strong interaction of nickel with the support favors the stability of the catalysts in the DRM reaction.

Introduction

The effects of global warming have prompted the search for technological alternatives to mitigate its impact and thus avoid the increase in greenhouse gas emissions, with CO_2 and CH_4 representing an important part of the total amount emitted into the atmosphere. Among these alternatives, the dry reforming of methane (DRM; $CO_2 + CH_4 \rightleftharpoons 2\,CO + 2H_2$) has been positioned as a technology that can reduce pollution while also acting as an important energy, source, thus allowing the development of a comprehensive system for capturing greenhouse gases [1].

Developing efficient catalysts that allow the application of DRM on an industrial scale is essential for the implementation of this technology and to produce synthesis gas that can be used to obtain synthetic gasoline [2]. As the support plays a key role in the catalytic activity, it must therefore be carefully selected to allow full advantage to be taken of its physical and chemical properties, such as texture, thermal stability, redox properties, storage capacity, oxygen, and surface acidity-basicity [3,4]. This improves the metal-support interaction and increases the dispersion of active metal particles, thus minimizing the effects of C deposition [5,6]. Noble metals such as Ir, Rh, Ru, Pt, and Pd have a higher resistance to coke deposition than non-noble metals. Given that noble metals are more expensive than non-noble metals, an inexpensive way to prevent coke formation involves the use of multi-metal formulations of non-noble metals such as Ni, Co, and Fe with noble metals [7]. These formulations facilitate metal dispersion and generate more active metallic centers [8]. Ni is the only transition metal that exhibits catalytic properties comparable to those of precious metals. However, Ni-based catalysts tend to generate carbon deposits on the catalyst surface and, subsequently, a loss of catalyst activity. The resulting poor stability limits the commercial use of Ni-based catalysts for DRM reactions and, therefore, Ni-based catalysts must be modified—in terms of the nature of the support and the preparation method—to improve their performance and resistance to carbon deposition [4,9,10].

Hexaaluminates are an excellent choice as DRM catalytic supports due to their thermal stability [11]—they exhibit high thermal resistance above 1873 K. The general formula for hexaaluminates is $AB_xAl_{12-x}O_{19}$, where AB represents a large cation such as Ba, La, Na, etc. and a transition (Co, Cu, Fe, Mn, Ni, etc.) or noble metal (Ir, Pd, Rh, Ru, etc.). These materials have been used as catalysts for high temperature applications, superionic conductors and luminescent laser materials, ceramics, and matrices for immobilization of radioactive elements, amongst others [12,13]. In recent years, several synthetic methods for the production of hexaaluminates have been developed, including lyophilization, nitrate decomposition, solid-state reaction, sol-gel, coprecipitation, inverse microemulsion, and hydrothermal synthesis [11]. The most widely used synthetic method is coprecipitation, in which the precursors are homogeneously mixed in the form of ions and precipitated simultaneously. In recent years, this method has been the object of studies aimed at improving the textural properties of the materials synthesized. In this regard, unconventional drying methods, as well as the use of nonconventional sources of raw materials, such as industrial inorganic waste, have been explored.

Wastes known as aluminum saline slags are generated during aluminum recycling. These slags contain metallic Al, various oxides, and flux brines as main components, with variations in the percentages thereof depending on the nature of the material to be recycled [14,15]. Due to their limitations for final disposal in controlled landfills, these slags have been used recently to synthesize various materials, including alumina, calcium aluminate, layered double hydroxides, molecular sieves, microporous aluminophosphate, zeolites, pillared clays, and hexaaluminates [15–34]. The objective of these works is to synthesize materials with an application and that, therefore, can contribute to the recovery of industrial waste. The objective of the work would be framed within the so-called *Circular Economy* [38]. Logically, it is necessary to compare these new materials with the materials that are being used in these applications, to reduce and control the new emissions of pollutants generated and, if they can be applied, to analyze economically this route of recovery of inorganic industrial waste.

In this work, a hibonite-type Ni/La-hexaaluminate synthesized from an industrial waste is used and compared as catalyst in DRM. The structure, catalytic behavior, and stability during a run time of at least 50 h of three Ni-catalysts obtained from two commercial supports and two preparation methods were used for comparison.

Experimental

Materials, reagents, gases, and aluminum extraction

Lanthanum(III) chloride heptahydrate (99.9%, Sigma-Aldrich), nickel(II) nitrate hexahydrate (99% Panreac), polyethylene glycol 400 (Merck), polyethylene glycol monolaurate 400 (PegMn400, Aldrich), and methanol (99.8%, ACS) were used as materials and reagents for the synthesis of the hexaaluminate

and supported catalysts. Carbon dioxide (99.996%, Praxair), helium (99.999%, Praxair), hydrogen (99.999%, Praxair), methane (99.5%, Praxair), and nitrogen (99.999%, Praxair) were also used in the characterization and catalytic-performance studies.

Aluminum was extracted from the saline slag using a previously reported procedure [33]; briefly, 50 g of saline slag was added to 750 mL of an aqueous reagent solution (HCl 2 mol/dm^3) in a reflux system consisting of a 1000 cm^3 Erlenmeyer flask with tube condenser, thus avoiding volume losses. The slurry was heated to 373 K and kept at that temperature for 2 h. The solution was then allowed to cool and separated by centrifugation. The most important constituents of the filtered solution were determined by ICP-OES using a VARIAN ICP-OES VISTA MPX with radial vision: Al (9.40 g/dm^3), Ca (1.19 g/dm^3), Fe (1.03 g/dm^3) and Si (0.33 g/dm^3).

The synthesis of La-hexaaluminate-support was performed with a La/Al molar ratio of 1:11 using a previously reported and optimized method [33]. The slag solution was concentrated to one third of its initial volume to obtain a yellow liquor. A microelmulsion was then prepared using Methanol/Peg400/PegMn400/Al solution in a volumetric ratio of 1/0.8/0.4/0.6. The lanthanum chloride was mixed with the aluminum solution at 353 K, with vigorous stirring. After 10 min, the methanol was added slowly, the mixture stirred for a further 10 min, then Peg400 and PegMn400 were added and the temperature increased to 373 K. This mixture was kept under these conditions for 20 min prior to digestion in the autoclave. The resulting final mixture was heated in a stainless steel autoclave at 493 K for 16 h, drying in an oven until the liquid matrix had been eliminated, then calcined at 673 K for 1 h and 1473 K for 2 h, in both cases using a heating ramp of 10 K/min (Ni/LHA). Wet impregnation of the La-hexaaluminate support synthesized was carried out using 10 wt% of NiO, then the catalyst with the impregnated metallic phase was calcined at 673 K for 2 h. For comparison, the same method is used to prepare the Ni/LHA catalyst but using aluminum nitrate nonahydrate (≥98%, sigma-Aldrich) as aluminum source [34]. Three reference catalysts were prepared using two methods, namely wet impregnation (I) and precipitation-deposition (PD), starting from two commercial oxides, γ-Al_2O_3 (Rhône-Poulenc) and SiO_2 (AF125, Kali Chemie), as supports (Ni–I/Al_2O_3, Ni–I/SiO_2 and Ni-PD/SiO_2) [39].

Characterization techniques

The structural phases were analyzed using an X-ray diffractometer (model Siemens D5000) equipped with a Ni-filtered CuKα radiation source (λ = 0.1548 nm). The main textural properties of the solids were determined by nitrogen adsorption at 77 K using two Micromeritics ASAP (2010 and 2020 Plus) adsorption analyzers. Prior to the adsorption measurements, 0.3 g of sample was degassed at 473 K for 2 h at pressures lower than 0.133 Pa. The BET surface area (S_{BET}) was calculated from the adsorption data obtained over the relative pressure range 0.05–0.20. The total pore volume (V_P) was calculated from the amount of nitrogen adsorbed at a relative pressure of 0.99. Temperature-programmed reduction (TPR) studies were performed using a Micromeritics TPR/TPD 2900 equipment instrument. TPR tests were then performed from room temperature to 1273 K under a total flow of 30 mL/min (5% H_2 in Ar, Praxair). Finally, the morphological analysis and chemical composition of the samples were carried out using a SEM Phenom XL desktop (Mode: 15 kV - Map, Detector: BSD Full) and HR-TEM (JEOL JEM 2100F, Accelerating voltage: 200 kV, Detector: X-Max).

Catalytic performance

DRM was carried out at 973 K using an automated bench-scale catalytic unit (Microactivity Reference, PID Eng&Tech). The reactor was a tubular, fixed-bed, downflow type, with an internal diameter of 0.9 cm and a length of 30 cm. Catalyst samples (25 mg) were mixed with an inert material (SiC, VWV Chemicals-Prolabo) to dilute the catalyst bed and avoid hot-spot formation. The reaction mixture consisted of CH_4 and CO_2 with a molar ratio of 1:1 (concentration of 12% in the feed), with helium as equilibrium gas up to a total feed flow of 40 cm^3/min, thus achieving a gas hourly space velocity (GHSV) of $9.6 \cdot 10^4$ cm^3/g h. Before the reaction, the catalyst was reduced *in situ* using 30 cm^3/min of H_2 at 973 K for 2 h. The reagent and product streams were analyzed using an Agilent 6890 gas chromatography system.

Results and discussion

The nitrogen adsorption isotherms for the supports and catalysts were of type II and IV in the BDDT classification [40] (see Fig. 1). The specific surface area (S_{BET}) and total pore volume (Vp) derived from the experimental adsorption results are summarized in Table 1. A decrease in textural parameters for the supported catalysts with respect to their corresponding support can be seen. In the case of the precipitation-deposition preparation method, reduction of the textural properties compared to the properties of the catalyst obtained by impregnation was not so important, and can be related to the formation of a talc-like nickel phyllosilicate structure during synthesis of the catalyst. This structure that is formed has been previously reported by our research group [41]. The incorporation of nickel through the wet impregnation method, and its subsequent drying and calcination to obtain NiO, causes the clogging of the porous structure. Under these conditions, the textural properties of the catalyst, specific surface area and pore volume are reduced, with a decrease from 304 to 225 m^2/g and from 0.840 to 0.615 cm^3/g. In the case of the precipitation-deposition preparation method, the textural properties are practically maintained to those corresponding to those of the support precisely due to the formation of the talc-like nickel phyllosilicate structure.

The XRD patterns of the supported nickel catalysts are presented in Fig. 2. In the case of the hexaaluminate, a very complex diffractogram was obtained. Based on the synthesis methods used and the presence of La and Ca, the most probable hexaaluminate structure appears to be magnetoplumbite (hibonite-Ca, pattern # 00-007-0785). The hexaaluminate obtained presents crystalline characteristics and different phases, as indicated in Fig. 2. The patterns of the samples prepared by wet impregnation reveal the presence of NiO. In

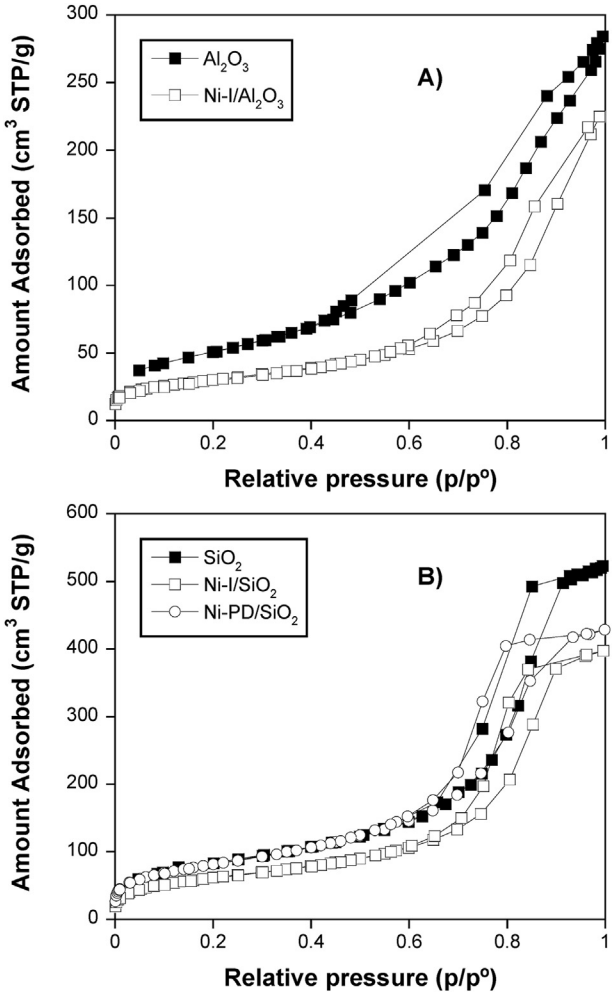

Fig. 1 – The N_2 adsorption-desorption results at −196 °C for: alumina based catalysts (A), and silica based catalysts (B).

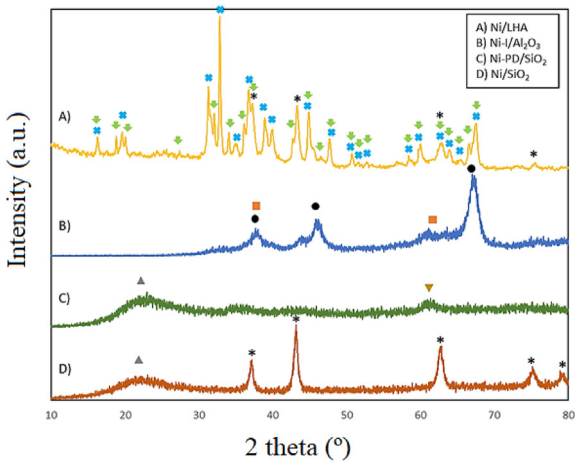

Fig. 2 – XRD patterns of Ni/LHA (A), Ni–I/Al_2O_3 (B), Ni-PD/SiO_2 (C) and Ni–I/SiO_2 (D).* = NiO-PCPDFWIN card, File 01-001-1239; = SiO_2-PCPDFWIN card, File 01-083-2470; = SiO_2-PCPDFWIN card, File 01-080-0369; = Al_2O_3-PCPDFWIN card, File 01-001-1308; = NiO-PCPDFWIN card, File 01-073-1519; = Al_2O_3 - PCPDFWIN card, File 00-035-0121; = $CaAl_{12}O_{19}$-PCPDFWIN card, File 01-076-0665.

Table 1 – Physico-chemical characteristics of the catalysts.

Sample	S_{BET} (m^2/g)	Vp (cm^3/g)	NiO (wt.%)	$d_{crystallite}$ (nm)
LHA	45	–	–	–
Ni/LHA	42	–	10	18.5
Al_2O_3	185	0.426	–	–
Ni–I/Al_2O_3	108	0.348	12.69	9.7
SiO_2	304	0.840	–	–
Ni-PD/SiO_2	296	0.663	4.79	40.4
Ni–I/SiO_2	225	0.615	9.12	25.2

the case of the hexaaluminate, the structure of the support remains perfectly stable, without modification. Logically, supports with a higher specific surface area will favor the dispersion of NiO, which can favor the catalytic behavior of these materials. The pattern of the sample prepared by the precipitation-deposition method corresponds mainly to that of the silica support. The possible formation of talc-like nickel phyllosilicate compounds has been reported previously [39,41]. The crystallite sizes of NiO determined using the Scherrer equation can be found in Table 1.

The TPR analysis provides information about the interaction between NiO and the support. Depending on the reduction temperatures, the degree of interaction of the NiO species can be classified into four different types: α, $\beta 1$, $\beta 2$ and γ [42]. The TPR patterns and TCD curves of the supported NiO catalysts are included and compared in Fig. 3. A comparison between the TPR data and the main regions of this classification has also been included in Fig. 3 A). The maximum peak temperatures and fraction of the total area represented by each can be found in Table 2. Fig. 3 also shows the deconvolution of overlapping peaks using a Gaussian fit for determination. In the case of Ni/LHA, a single peak appears and then undergoes a complete reduction in the region of weak or poor NiO/support intercations, representing 100% of the total peak area. The peak found is not totally symmetric (maximum reduction temperatures at 612 and 652 K), thus suggesting that two types of NiO particles are present and that they may interact with a different surface that makes their reduction rate slightly different. A reduction behavior similar to the previous one can be seen in the case of Ni–I/SiO_2, but in this case it also encompasses the next interaction stage ($\beta 1$). This behavior could be related to NiO particles dispersed on the surface of the easily reducible support (651 K) and other particles occluded in the porous structure, which are more difficult to reduce. The area of the first peak corresponds to 44%, whereas the other peak accounts for 56% of the total. A shift of the TPR peaks to higher temperatures is observed for the samples prepared by the precipitation-deposition method (NiO-PD/SiO_2) and considering Al_2O_3 as support. In these two cases the temperatures of the reduction maxima are shifted to 871 and 981–1044 K, respectively. These catalysts exhibit four peaks with maximum peak area percentages of 71% (Ni-PD/SiO_2) and 74% (Ni–I/Al_2O_3) in the interaction stages $\beta 1$ and $\beta 2$. The main

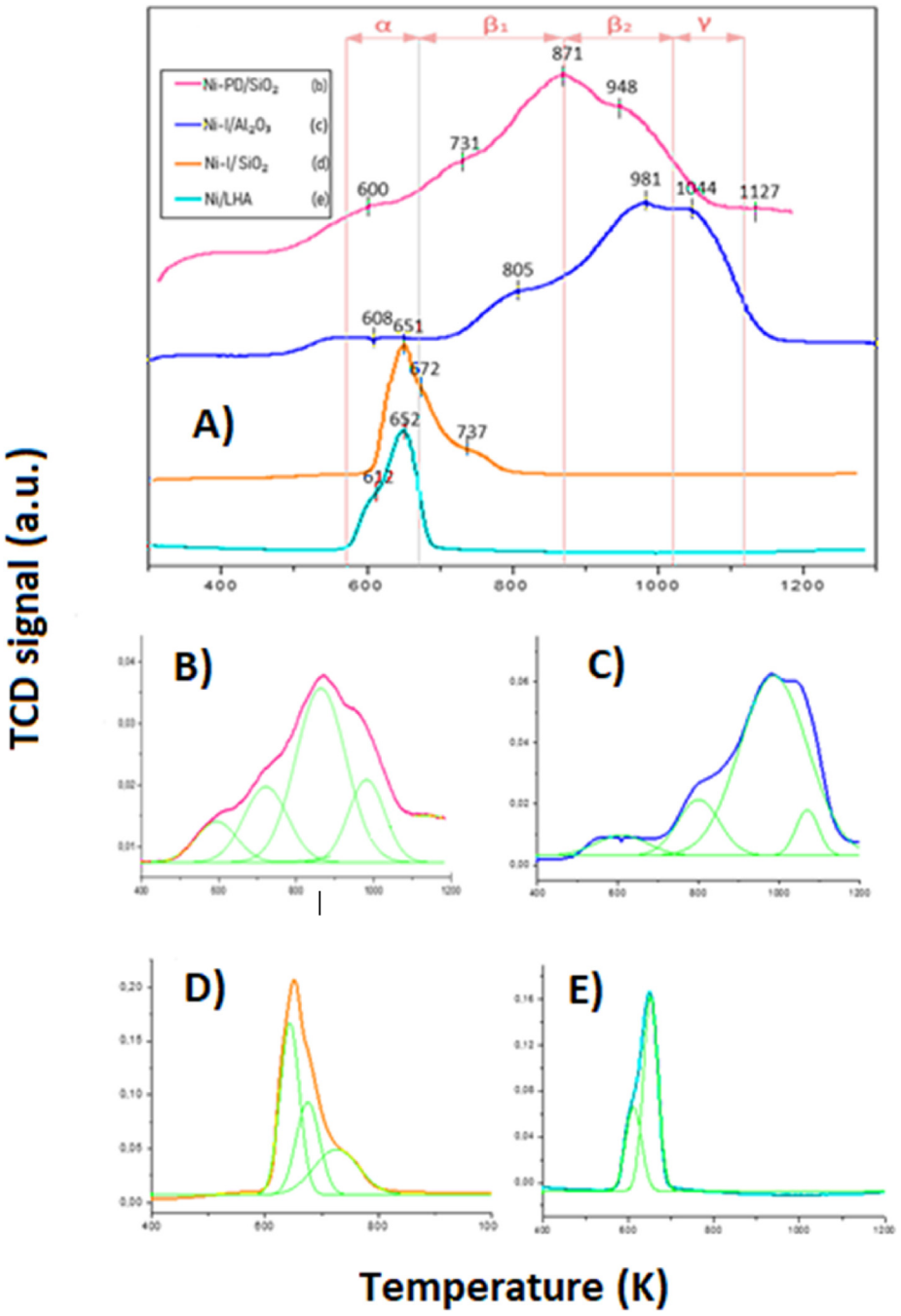

Fig. 3 – TPR patterns of the nickel oxide-supported catalysts calcined at 823 K (A). Peak deconvolution for Ni-PD/SiO_2 (B). Peak deconvolution for Ni–I/Al_2O_3 (C). Peak deconvolution for Ni–I/SiO_2 (D). Peak deconvolution for Ni/LHA (E).

Table 2 – Maximum temperature and fraction of the peak areas of the TPR curves for the catalyst.

Catalyst	Tmax (K); Peak area fraction (%)							
	α		β1		β2		γ	
Ni–I/SiO_2	651, 672	44, 29	737	27	–	–	–	–
Ni–I/Al_2O_3	608	6	805	14	981	74	1044	6
Ni-PD/SiO_2	605	3	730, 865	9, 71	948	17	–	–
Ni/HLA	612; 652	32; 68	–	–	–	–	–	–

difference between the two catalysts is that the reduction temperatures found for the Ni–I/Al_2O_3 catalyst are shifted to a higher temperature. Indeed, the highest temperature of one of the reduction peaks in this case is 1044 K. These results confirm the findings of the X-ray structural analyses, namely that the formation of various nickel compounds makes it more difficult to reduce than the NiO metallic oxide. These results are in according to the degree of interaction/reaction of nickel with the surface of the SiO_2 and Al_2O_3 supports, aspects previously referenced in the literature [41]. The structure of γ-alumina and the size of Ni^{2+} allow the formation of Ni–Al spinel, especially if it favors temperature. Under these conditions, the reduction temperature of nickel increases considerably when compared to the reduction of NiO particles dispersed on a support. This is the situation observed in Ni–I/LHA and Ni–I/SiO_2. When the preparation method is modified so that the degree of nickel interaction with the support surface (Ni-PD/SiO_2) increases, the reduction temperature also increases, precisely because of the presence of this strong interaction.

Catalytic performance

The DRM reaction ($CO_2 + CH_4 \rightleftharpoons 2\,CO + 2H_2$) is affected by several parallel reactions that occur during the catalytic process: methane decomposition ($CH_4 \rightleftharpoons C + 2H_2$), the reverse water-gas shift reaction (RWGS; $CO_2 + H_2 \rightleftharpoons CO + H_2O$), the Boudouard reaction ($2\,CO \rightleftharpoons C + CO_2$), CO_2 hydrogenation ($CO_2 + 2H_2 \rightleftharpoons C + 2H_2O$), CO hydrogenation ($CO + H_2 \rightleftharpoons C + H_2O$), and steam reforming ($CH_4 + H_2O \rightleftharpoons CO + 3H_2$). The conversion and ratio of CO_2 and CH_4, as well as the selectivity with respect to hydrogen (H_2/CO), can give an idea of the prevalence of these reactions during DRM.

The conversion (CO_2–CH_4), selectivity (H_2/CO), and carbon balance (CB) results obtained for the catalysts during a long 50 h catalytic test are presented in Fig. 4. The carbon dioxide and methane conversions $[X]_i$, selectivity [H_2/CO] and carbon balance (CB) were calculated using the following equations:

$$[X]_{CH_4} = \frac{[CH_4]_{in} - [CH_4]_{out}}{[CH_4]_{in}} \quad \text{Equation 1}$$

$$[X]_{CO_2} = \frac{[CO_2]_{in} - [CO_2]_{out}}{[CO_2]_{in}} \quad \text{Equation 2}$$

$$Selectivity\left[\frac{H_2}{CO}\right] = \frac{\frac{[H_2]_{out}}{2*[CH_4]_{in}}}{\frac{[CO]_{out}}{[CH_4]_{in}+[CO_2]_{in}}} \quad \text{Equation 3}$$

$$CB = \frac{[CO_2]_{out} + [CO]_{out} + [CH_4]_{out}}{[CH_4]_{in} + [CO_2]_{in}} \quad \text{Equation 4}$$

In the case of Ni–I/SiO_2, this catalyst showed a very different thermodynamic behavior from the rest, with the conversion of CH_4 and CO_2 and selectivity decreasing during the DRM reaction, with slopes of $\Delta X_{CO2} \approx -\ 6\,\%$, $\Delta X_{CH4} \approx -\ 14\,\%$, $\Delta X_{CH4} \approx -\ 7\,\%$ (see Fig. 4 A) B) C)) and, therefore, an increasing slope for the CB during the first 35 h (3%), subsequently stabilizing to a mean value of 98%. This behavior can be related to a high deposition of coke, which explains the low catalytic performance as a result of deactivation of the catalyst at a

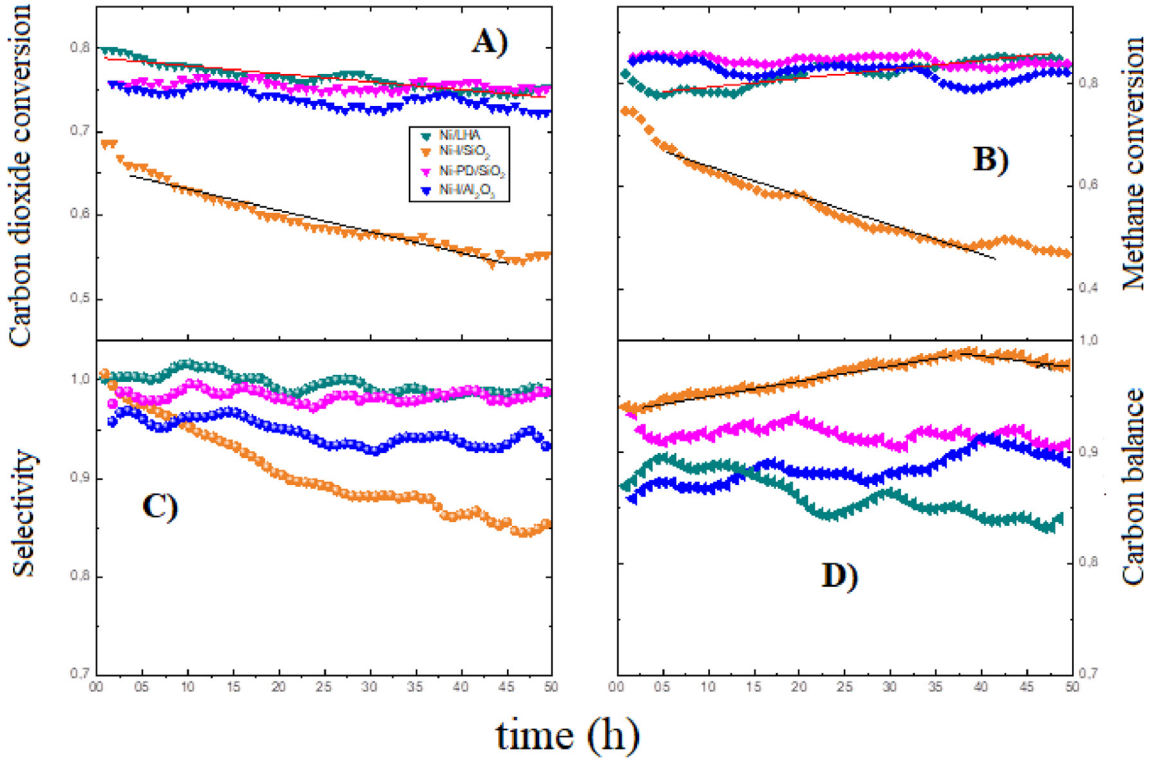

Fig. 4 – CO_2 conversion (A). CH_4 conversion (B). H_2/CO selectivity (C). Carbon balance, to differents catalyst in DRM at 973 K for 50 h (D).

constant rate, practically during the entire test run. The blocking effect of the active sites could be attributed to the morphological transformations that the support and metallic phase undergo during the reduction stage, as an effect of a weak interaction (type α) in which the nickel nanoparticles are practically free and/or weakly fixed on SiO_2. This situation causes a high rate of diffusive migration on the surface of the catalyst, thereby greatly benefiting the sintering and growth of the NiO grains. This effect is induced by the thermal gradient and the differences between the calcination and reduction temperature before the DRM test, as well as the impregnation method used for deposition of the metallic phase. In the case of Ni-PD/SiO_2 and Ni–I/Al_2O_3, the catalytic behavior of these catalysts is much more stable than for Ni–I/SiO_2, with a slight increase in the case of Ni-PD/SiO_2 with respect to Ni–I/Al_2O_3. The CO_2 conversion presents mean values of between 73% and 75% (see Fig. 4 A)). The CH_4 conversion also maintains the same thermodynamic regime for both catalysts with average values of between 82% and 85%. With regard to the H_2/CO selectivity (see Fig. 4C)), Ni-PD/SiO_2 presents an average value of 98% versus 94% for Ni–I/Al_2O_3, and in the case of the CB (see Fig. 4 D)), in the first 40 h they show different behaviors, with Ni–I/Al_2O_3 presenting an increasing behavior, stopping at 85% and stabilizing at around 95%, whereas Ni-PD/SiO_2 remains at around a mean value of 98%. Over the last 10 h, both catalysts essentially stabilize in the same thermodynamic regime. The precipitation-deposition method (PD) allows a significant improvement in the catalytic performance for Ni-PD/SiO_2 compared to Ni–I/SiO_2. These results seem to indicate that the strong interaction of nickel with the support favors the stability of the DRM reaction. The hexaaluminate catalyst (Ni/LHA) exhibited the best catalytic performance in terms of yield and stability, with CO_2 conversion values of 80% at the beginning of the reaction and 75% at the end ($\Delta X = -2\%$). CH_4 (opposite behavior to that of CO_2), in turn, presents an increasing slope of 4% up to a final value of 85%, a behavior which is better than that of the aforementioned catalysts at all times (see Fig. 4 A), B)). With regard to H_2/CO selectivity and CB (see Fig. 4C), D)), Ni/LHA continues to show a consistent thermodynamic behavior, with mean H_2/CO selectivity values of 99% and a CB of 76%, thus exhibiting the best H_2/CO ratio and the lowest rate of deactivation by coke deposition. Similarly to the strong interaction of nickel with the support, the presence of Al in the catalyst also seems to favor the stability of the reaction.

SEM, TEM, and TEM-HAADF images for NiO/LHA are shown in Fig. 5 before the reduction stage and after the catalytic test. The morphology of the catalyst (see Fig. 5 A) and B)) shows spherical agglomerates of NiO/LHA for the fresh catalyst and a rosette-like morphology for the used catalyst. The carbonaceous deposits generated during DRM, which were identified as filamentous carbon and carbon nanotubes (see Fig. 5 B) E)) that displace the Ni^0 grains (distribution in the range dp ≈ 10–50 nm, see Fig. 5 F)) from the catalyst surface, are also found. Although these forms of coke still block the active

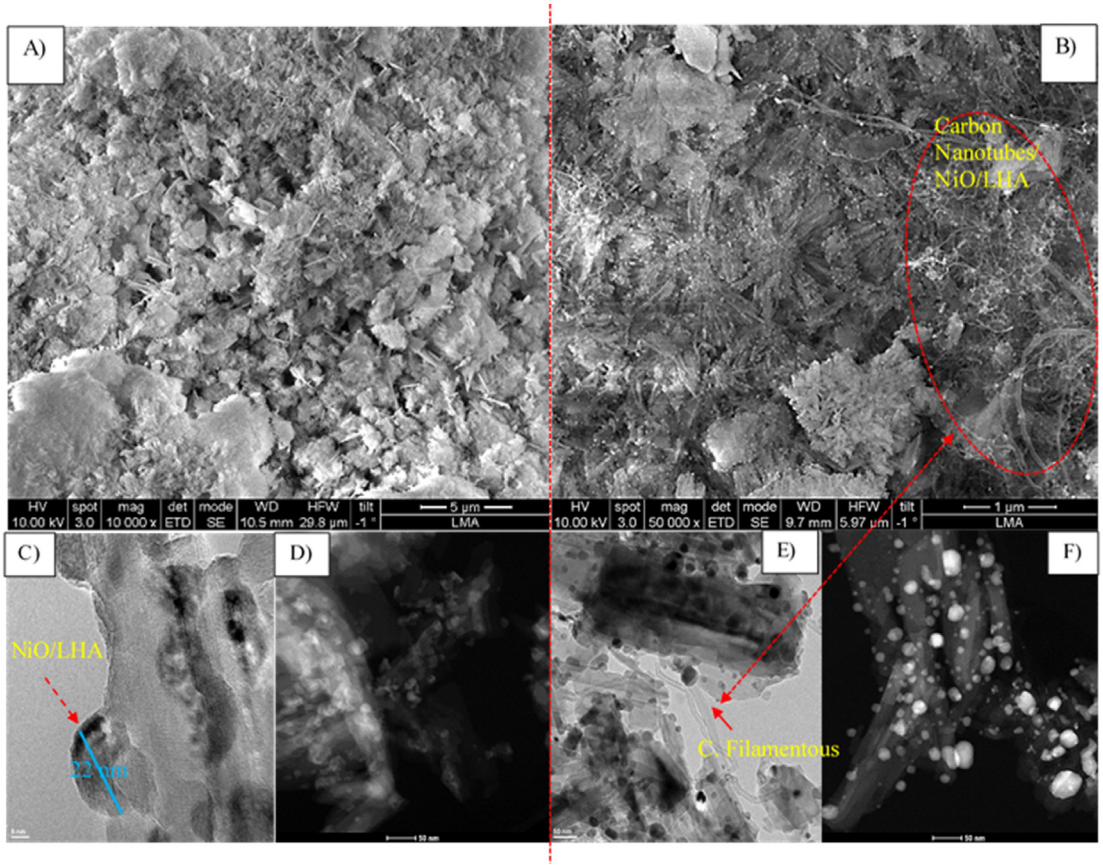

Fig. 5 – SEM, TEM and TEM-HAADF images of NiO/LHA catalyst fresh and used after 50 h in DRM at 973 K. Fresh catalyst [A)-SEM, C)-TEM, D)-TEM_HAADF]; used catalyst [B)-SEM, E)-TEM, F)-TEM_HAADF].

metallic sites, they are the least harmful, thus allowing this catalyst to maintain great stability and excellent performance in DRM at 973 K. Another important aspect to highlight is that the amount of carbon produced is much lower than the critical concentration necessary to completely exhaust the catalyst and cause it to lose its catalytic ability compared to other catalysts, which in turn exhibit better textural properties.

Conclusion

A Ni/La-hexaaluminate catalyst has been synthesized using an aluminum saline slag—a hazardous waste generated in aluminum recycling—as aluminum source in the synthesis of the La-hexaaluminate used as catalytic support. The catalysts were synthesized by impregnation. This method generated two types of morphologies, namely rosettes and clusters of amorphous tables, which allow a good distribution of the metallic nanoparticles on the support, as determined by SEM and HR-TEM. The catalyst showed excellent stability after 50 h of DRM reaction at 973 K. The conversion of CH_4 is higher than CO_2 and the H_2/CO selectivity is about 99%, thus suggesting the predominance of the Boudouard reaction over the RWGS reaction. The behavior of this catalyst is comparable to that of Ni–I/Al_2O_3 and Ni-PD/SiO_2, which is related to both the Ni-support interaction and the presence of alumina.

Author contributions

All the authors conceived, designed, and performed the experiments, analyzed the data, and drafted the manuscript.

Declaration of competing interest

The authors declare that they have no known competing financial interests or personal relationships that could have appeared to influence the work reported in this paper.

Acknowledgements

The authors are grateful for financial support from the Spanish Ministry of Science and Innovation (MCIN/AdslEI/10.13039/501100011033) through project PID2020-112656RB-C21. JJTH thanks Universidad Pública de Navarra for a postdoctoral grant. AG also thanks Santander Bank for funding via the Research Intensification Program.

REFERENCES

[1] Chen Y, Li M, Li Z, Liu F, Song G, Kawi S. Efficient syngas production via CO_2 reforming and electroreduction reactions through catalyst design. Energy Convers Manag 2022;265:115744. https://doi.org/10.1016/j.enconman.2022.115744.

[2] Li Z, Lin Q, Li M, Cao J, Liu F, Pan H, Wang Z, Kawi S. Recent advances in process and catalyst for CO_2 reforming of methane. Renew Sustain Energy Rev 2020;134:110312. https://doi.org/10.1016/j.rser.2020.110312.

[3] Li Z, Das S, Hongmanorom P, Dewangan N, Wai MH, Kawi S. Silica-based micro- and mesoporous catalysts for dry reforming of methane. Catal Sci Technol 2018;8:2763–78. https://doi.org/10.1039/C8CY00622A.

[4] Torrez-Herrera JJ, Korili SA, Gil A. Recent progress in the application of Ni-based catalysts for the dry reforming of methane. Catal Rev Sci Eng 2021. https://doi.org/10.1080/01614940.2021.2006891 (in press).

[5] Frontera P, Macario A, Aloise A, Antonucci PL, Giordano G, Nagy JB. Effect of support surface on methane dry-reforming catalyst preparation. Catal Today 2013;218–219:18–29. https://doi.org/10.1016/j.cattod.2013.04.029.

[6] Aramouni NAK, Touma JG, Tarboush BA, Zeaiter J, Ahmad MN. Catalyst design for dry reforming of methane: analysis review. Renew Sustain Energy Rev 2018;82:2570–85. https://doi.org/10.1016/j.rser.2017.09.076.

[7] Torrez-Herrera JJ, Korili SA, Gil A. Bimetallic (Pt-Ni) La-hexaaluminate catalysts obtained from aluminum saline slags for the dry reforming of methane. Chem Eng J 2022;433:133191. https://doi.org/10.1016/j.cej.2021.133191.

[8] Mortensen PM, Dybkjær Ib. Industrial scale experience on steam reforming of CO_2-rich gas. Appl Catal A-Gen 2015;495:141–51. https://doi.org/10.1016/j.apcata.2015.02.022.

[9] Salaev MA, Liotta LF, Vodyankina OV. Lanthanoid-containing Ni-based catalysts for dry reforming of methane: a review. Int J Hydrogen Energy 2022;47:4489–535. https://doi.org/10.1016/j.ijhydene.2021.11.086.

[10] Mo W, Ma F, Ma Y, Fan X. The optimization of Ni-Al_2O_3 catalyst with the addition of La_2O_3 for CO_2-CH_4 reforming to produce syngas. Int J Hydrogen Energy 2019;44:24510–24. https://doi.org/10.1016/j.ijhydene.2019.07.204.

[11] Torrez-Herrera JJ, Korili SA, Gil A. Progress in the synthesis and applications of hexaaluminate-based catalysts. Catal Rev Sci Eng 2022;64:592–630. https://doi.org/10.1080/01614940.2020.1831756.

[12] Zhu Y, Liu R, Sun X, Ma X, Wang X, Tian H. Metal modified hexaaluminates for syngas generation and CO_2 utilization via chemical looping. Int J Hydrogen Energy 2019;44:10218–31. https://doi.org/10.1016/j.ijhydene.2019.02.187.

[13] Xu L, Miao Z, Song H, Chou L. CO_2 reforming of CH_4 over rare earth elements functionalized mesoporous Ni–Ln (Ln = Ce, La, Sm, Pr)–Al–O composite oxides. Int J Hydrogen Energy 2014;39:3253–68. https://doi.org/10.1016/j.ijhydene.2013.12.077.

[14] Gil A. Management of the salt cake from secondary aluminum fusion processes. Ind Eng Chem Res 2005;44:8852–7. https://doi.org/10.1021/ie050835o.

[15] Gil A, Korili SA. Management and valorization of aluminum saline slags: current status and future trends. Chem Eng J 2016;289:74–84. https://doi.org/10.1016/j.cej.2015.12.069.

[16] Gil A, Arrieta E, Vicente MA, Korili SA. Synthesis and CO_2 adsorption properties of hydrotalcite-like compounds prepared from aluminum saline slag wastes. Chem Eng J 2018;334:1341–50. https://doi.org/10.1016/j.cej.2017.11.100.

[17] Gil A, Arrieta E, Vicente MA, Korili SA. Application of industrial wastes from chemically treated aluminium saline slags as adsorbents. ACS Omega 2018;3:18275–84. https://doi.org/10.1021/acsomega.8b02397.

[18] Galindo R, López-Delgado A, Padilla I, Yates M. Synthesis and characterisation of hydrotalcites produced by an aluminium hazardous waste: a comparison between the use of ammonia and the use of triethanolamine. Appl Clay Sci 2015;115:115–23. https://doi.org/10.1016/j.clay.2015.07.032.

[19] Galindo R, López-Delgado A, Padilla I, Yates M. Hydrotalcite-like compounds: a way to recover a hazardous waste in the

aluminium tertiary industry. Appl Clay Sci 2014;95:41–9. https://doi.org/10.1016/j.clay.2014.03.022.
[20] Santamaría L, López-Aizpún M, García-Padial M, Vicente MA, Korili SA, Gil A. Zn-Ti-Al layered double hydroxides synthesized from aluminum saline slag wastes as efficient drug adsorbents. Appl Clay Sci 2020;187:105486. https://doi.org/10.1016/j.clay.2020.105486.
[21] Santamaria L, Devred F, Gaigneaux EM, Vicente MA, Korili SA, Gil A. Effect of the surface properties of Me^{2+}/Al layered double hydroxides synthesized from aluminium saline slag wastes on the adsorption removal of drugs. Microporous Mesoporous Mater 2020;309:110560. https://doi.org/10.1016/j.micromeso.2020.110560.
[22] Santamaria L, Vicente MA, Korili SA, Gil A. Saline slag waste as an aluminum source for the synthesis of Zn-Al-Fe-Ti layered double-hydroxides as catalysts for the photodegradation of emerging contaminants. J Alloys Compd 2020;843:156007. https://doi.org/10.1016/j.jallcom.2020.156007.
[23] Santamaria L, Oliveira García L, de Faria EH, Ciuffi KJ, Vicente MA, Korili SA, Gil A. M(II)-Al-Fe layered double hydroxides synthesized from aluminum saline slag wastes and catalytic performance on cyclooctene oxidation. Miner Eng 2022;180:107516. https://doi.org/10.1016/j.mineng.2022.107516.
[24] Kuroki S, Hashishin T, Morikawa T, Yamashita K, Matsuda M. Selective synthesis of zeolites A and X from two industrial wastes: crushed stone powder and aluminum ash. J Environ Manag 2019;231:749–56. https://doi.org/10.1016/j.jenvman.2018.10.082.
[25] Belviso C, Kharchenko A, Agostinelli E, Cavalcante F, Peddis D, Varvaro G, Yaacoub N, Mintova S. Red mud as aluminium source for the synthesis of magnetic zeolite. Microporous Mesoporous Mater 2018;270:24–9. https://doi.org/10.1016/j.micromeso.2018.04.038.
[26] Sanchez Hernandez R, López-Delgado A, Padilla I, Galindo Llorach R, López-Andrés S. One-step synthesis of NaP1, SOD and ANA from a hazardous aluminum solid waste. Microporous Mesoporous Mater 2016;226:267–77. https://doi.org/10.1016/j.micromeso.2016.01.037.
[27] Hiraki T, Nosaka A, Okinaka N, Akiyama T. Synthesis of zeolite-X from waste metals. ISIJ Int 2009;49:1644–8. https://doi.org/10.2355/isijinternational.49.1644.
[28] Yoldi M, Fuentes-Ordoñez EG, Korili SA, Gil A. Zeolite synthesis from aluminum saline slag waste. Powder Technol 2020;366:175–84. https://doi.org/10.1016/j.powtec.2020.02.069.
[29] Jiménez A, Misol A, Morato A, Rives V, Vicente MA, Gil A. Synthesis of pollucite and analcine zeolites by recovering aluminium from a saline slag. J Clean Prod 2021;297:126667. https://doi.org/10.1016/j.jclepro.2021.126667.
[30] Cardona Y, Korili SA, Gil A. A nonconventional aluminum source in the production of alumina-pillared clays for the removal of organic pollutants by adsorption. Chem Eng J 2021;425:130708. https://doi.org/10.1016/j.cej.2021.130708.
[31] Cardona Y, Wegrzyn A, Miskowiec P, Korili SA, Gil A. Catalytic photodegradation of organic compounds using TiO_2/pillared clays synthesized using a nonconventional aluminum source. Chem Eng J 2022;446:136908. https://doi.org/10.1016/j.cej.2022.136908.
[32] Torrez-Herrera JJ, Fuentes-Ordoñez EG, Korili SA, Gil A. Evidence for the synthesis of La-hexaaluminate from aluminum-containing saline slag wastes: correction of structural defects and phase purification at low temperature. Powder Technol 2021;377:80–8. https://doi.org/10.1016/j.powtec.2020.08.087.
[33] Torrez-Herrera JJ, Korili SA, Gil A. Structure and activity of nickel supported on hibonite-type La-hexaaluminates synthesized from aluminum saline slags for the dry reforming of methane. Chem Eng J Adv 2021;5:100080. https://doi.org/10.1016/j.ceja.2020.100080.
[34] Torrez-Herrera JJ, Korili SA, Gil A. Effect of the synthesis method on the morphology, textural properties and catalytic performance of La-hexaaluminates in the dry reforming of methane. J Environ Chem Eng 2021;9:105298. https://doi.org/10.1016/j.jece.2021.105298.
[35] Li M, Ye Ch, Li Z, Lin Q, Cao J, Liu F, Song G, Kawi S. 1D confined materials synthesized via a coating method for thermal catalysis and energy storage applications. J Mater Chem 2022;10:6330–50. https://doi.org/10.1039/D1TA10540J.
[36] Li M, Li Z, Lin Q, Cao J, Liu F, Kawi S. Synthesis strategies of carbon nanotube supported and confined catalysts for thermal catalysis. Chem Eng J 2022;431:133970. https://doi.org/10.1016/j.cej.2021.133970. 2022.
[37] Li Z, Li M, Bi Z, Kathiraser Y, Kawi S. Design of highly stable and selective core/yolk–shell nanocatalysts—a review. Appl Catal, B 2016;188:324–41. https://doi.org/10.1016/j.apcatb.2016.01.067.
[38] Gil A. Challenges on waste-to-energy for the valorization of industrial wastes: electricity, heat and cold, bioliquids and biofuels. Environ Nanotechnol Monit Manag 2022;17:100615. https://doi.org/10.1016/j.enmm.2021.100615.
[39] Gómez-Polo C, Gil A, Korili SA, Pérez-Landázabal JI, Recarte V, Trujillano R, Vicente MA. Effect of the metal support interactions on the physicochemical and magnetic properties of Ni catalysts. J Magn Magn Mater 2007;316:e783–6. https://doi.org/10.1016/j.jmmm.2007.03.088.
[40] Gregg SJ, Sing KSW. Adsorption surface area and porosity. London: Academic Press; 1991.
[41] Gil A, Díaz A, Montes M. Passivation and reactivation of nickel catalysts. J Chem Soc Faraday Trans 1991;87:791–5. https://doi.org/10.1039/FT9918700791.
[42] Zhang J, Xu H, Jin X, Ge Q, Li W. Characterizations and activities of the nano-sized Ni/Al_2O_3 and $Ni/La\text{-}Al_2O_3$ catalysts for NH_3 decomposition. Appl Catal A-Gen 2005;290:87–96. https://doi.org/10.1016/j.apcata.2005.05.020.